Multi-period Electrical Array Reconfiguration for Multi-PV Systems Considering Net Power Fluctuation Mitigation

Mengyuan Wang, Xiaoyuan Xu, Shuai Fan, Zheng Yan, Bo Yang, and Xinping Guan

***Abstract*—The electrical array reconfiguration (EAR) method has become a promising solution to enhance photovoltaic (PV) system performance under partial shading conditions. Existing studies focus on maximizing single-period PV generation but neglect the impact of power fluctuation on grid stability. To address this, we propose a multi-period EAR method for multi-PV systems considering net power fluctuation mitigation. First, we design a multi-period EAR model to maximize total revenue by balancing electricity sales and net power fluctuation penalties, formulated as a stochastic mixed-integer quadratic programming problem. The model incorporates constraints on the average number of switching actions per unit time to ensure practical implementation. Then, to handle the unpredictability of partial shading conditions, we develop a Lyapunov optimization-based online algorithm to decouple the time-coupling constraints involving state transitions. Additionally, we propose a reduced set of EAR strategies to improve the computational efficiency. Numerical studies demonstrate that the proposed method significantly reduces net power fluctuations in distribution networks with high PV penetration rate and enhances total revenue compared with conventional methods.**

***Index Terms*—Distribution network, photovoltaic (PV), partial shading, grid stability, electrical array reconfiguration (EAR), power fluctuation, mixed-integer quadratic programming, Lyapunov optimization.**

Nomenclature

A. Indices

a_i	Index of electrical array reconfiguration (EAR) strategy for photovoltaic (PV) i
i	Index of PV array
j_i	Index of modules of PV i
m_i	Index of columns of PV i
n_i	Index of rows of PV i
t	Index of time slots
w_i	Index of power peaks of PV i

B. Parameters

α	Coefficient designed to penalize fluctuation of net power between two time slots
η	Queue-update step size
π^t	Electricity sales price at time slot t
A_i	Number of EAR strategies in $\boldsymbol{S}_i^t$
G_0	Solar irradiance under standard test condition (STC) (G_0=1000 W/m^2)
I	Number of PV arrays
$I_{m,i}$	Operating current of a module of PV i under STC
J_i	Number of modules of PV i
M_i	Number of rows of PV i
N_i	Number of columns of PV i
$P_{PV,i}$	Capacity of PV i
Q	Average number of switches at every time slot
$\boldsymbol{S}_i^t$	Vector of EAR strategies of PV i at time slot t
$V_{m,i}$	Operating voltage of a module of PV i under STC

C. Variables

$\boldsymbol{\Theta}^t$	Vector of random variables in multi-period EAR problem $\mathbb{P}_1$
$\tilde{A}_i^t$	Number of EAR strategies in $\tilde{\boldsymbol{S}}_i^t$
$\boldsymbol{G}_i^t$	Irradiance distribution of PV i at time slot t ($\boldsymbol{G}_i^t \in \mathbb{R}^{m_i \times n_i}$)
G_{i,m_i,n_i}^t	Element of $\boldsymbol{G}_i^t$ in row m_i and column n_i
G_{r,i,m_i}^t	Total irradiance on modules in row m_i of PV i at time slot t
$\boldsymbol{H}^t$	Vector of virtual queues at time slot t
H_i^t	Virtual queue of Lyapunov optimization-based online distributed (LOOD) algorithm at time slot t

Manuscript received: July 22, 2024; revised: November 1, 2024; accepted: February 7, 2025. Date of CrossCheck: February 7, 2025. Date of online publication: February 26, 2025.

This work was supported by the Shanghai Science and Technology Plan Project (No. 23DZ1201200) and National Natural Science Foundation of China (No. 52477110).

M. Wang, X. Xu (corresponding author), S. Fan, and Z. Yan are with the Ministry of Education, Key Laboratory of Control of Power Transmission and Conversion (Shanghai Jiao Tong University), Shanghai 200240, China, and they are also with the Shanghai Non-carbon Energy Conversion and Utilization Institute, Shanghai 200240, China (e-mail: wangmy@sjtu.edu.cn; xuxiaoyuan@sjtu.edu.cn; fanshuai@sjtu.edu.cn; yanz@sjtu.edu.cn).

B. Yang and X. Guan are with the Department of Automation, Shanghai Jiao Tong University, Shanghai 200240, China (e-mail: bo.yang@sjtu.edu.cn; xpguan@sjtu.edu.cn).

DOI: 10.35833/MPCE.2024.000779

I^t_{r,i,m_i}	Current limitation of each row of PV i at time slot t
I^t_{m,i,w_i}	Current at w_i of PV i at time slot t
m^t_{r,i,w_i}	Number of rows with a total irradiance G^t_{r,i,w_i}
P^t_0	Net power output at time slot t
$P^t_{c,i}$	Curtailment of PV i at time slot t
P^t_d	Load demand at time slot t
P^t_{m,i,w_i}	Power at w_i of PV i at time slot t
$P^t_{sm,i}$	The maximum power output of PV i at time slot t
s	Number of different total irradiances on modules in rows of PV i at time slot t
$\boldsymbol{S}^t_{i,a_i}$	Vector of EAR strategies a_i of PV i at time slot t
S^t_{i,a_i,j_i}	Electrical position of module located at physical location j_i in $\boldsymbol{S}^t_{i,a_i}$
$\boldsymbol{S}^{t,*}_i$	Vector of optimal EAR strategies of PV i at time slot t
$\tilde{\boldsymbol{S}}^t_i$	Matrix of EAR strategies of PV i after reduced by two rules at time slot t
$\boldsymbol{u}^t_i$	Vector of indicators of EAR strategies in $\boldsymbol{S}^t_i$
u^t_{i,a_i}	The a_i^{th} element of $\boldsymbol{u}^t_i$
V^t_{m,i,w_i}	Voltage at w_i of PV i at time slot t

I. Introduction

PHOTOVOLTAIC (PV) technology has seen rapid growth globally in the last decade, from small rooftop installations to multi-megawatt PV power plants [1]. Various studies have shown that environmental factors such as cloud cover, power lines, trees, and buildings can cause partial shading conditions (PSCs) on PV arrays, leading to power fluctuations and drops in PV generation [2]-[4]. As a promising renewable energy option, the performance of PV systems under PSCs has an increasing impact on power system operation [5]-[7].

Recently, the PV array reconfiguration technique has been proposed to improve the performance of PV systems under PSCs. The mismatch loss of the PV systems under PSC is reduced, thereby increasing the PV generation [8]. This technique can be divided into static array reconfiguration and electrical array reconfiguration (EAR) methods [9]. Static array reconfiguration method involves the physical rearrangement of PV modules, which has inherent limitations in adapting to dynamic PSCs [10].

The EAR method mitigates the impact of the uneven irradiance on a PV array by dynamically modifying electrical connections between PV modules. This is achieved through an electrical switching matrix and supplementary circuits installed between the PV array and the inverter. Most existing EAR methods are based on the principle of "irradiance equalization", which aims to achieve uniformity in the row currents [11]- [14]. This principle is first proposed in [15], where PV modules are selectively connected in parallel to specific rows through the switching matrix based on their irradiance levels, thereby equalizing the available power across series-connected rows. Several opportunities are identified in [16] for further optimizing an irradiance equalization of dynamic PV array, indicating that smaller granularity systems have even greater potential. Reference [17] formulates the EAR problem as a mixed-integer quadratic programming (MIQP) problem using an irradiance level mismatch index to minimize mismatch losses. Many similar research works propose different optimization algorithms to enhance performance of the EAR, such as genetic algorithm [18], [19], particle swarm optimization [20], coyote algorithm [21], butterfly optimization algorithm [22], multi-objective grey wolf optimizer [23], marine predators algorithm [24], population-based algorithm [25], and grasshopper optimization algorithm [26]. The above algorithms perform reconfiguration on all modules in a PV array, while [27] proposes a different method where a PV array is divided into reconfigurable and fixed parts, conducting EAR only on the reconfigurable part to enhance the overall power output. Similar research works can also be found in [13] and [28], where different methods are employed to generate EAR strategies for the reconfigurable part. Reference [16] indicates that even simple EAR-enabled PV arrays can achieve 10% efficiency improvements over a conventional PV array, potentially reducing the return on investment by years in a real installation.

Although existing studies have demonstrated the effectiveness of EAR in mitigating the impact of PSCs, most research works only focus on the optimization of electrical connections between PV modules during a single period, while neglecting the long-term stochastic fluctuations of PV power output under PSCs and their alignment with grid operation demands [29], [30]. This can result in voltage fluctuations at the point of common coupling, increased stress on voltage regulation equipment, power quality issues affecting nearby loads, potential grid stability concerns, and increased requirements for reserve capacity in distribution networks [31]. Therefore, it is necessary to develop multi-period EAR methods to simultaneously improve PV generation and align power fluctuations with grid operation demands. Compared with traditional EAR methods that focus on single-period optimization to increase PV generation. The multi-period EAR method faces the following challenges.

1) The complex variations in load and irradiance distribution over long periods transform this problem into a stochastic mixed-integer nonlinear programming problem. Traditional methods for solving such problems, e.g., model predictive control [32] and stochastic programming [33], rely on predictable models, while the irradiance distribution on a PV array is inherently unpredictable.

2) This method requires an analytical expression for the PV power output under PSCs, which is challenging to derive due to the multiple peaked power-voltage characteristics caused by bypass diodes.

3) Existing methods minimize the number of switching actions during a single period [34], [35] without ensuring that the average number of switching actions is within the limit.

This paper proposes a multi-period EAR method for multi-PV systems considering net power fluctuation mitigation. The main contributions can be summarized as follows.

1) An optimization model is proposed that maximizes the long-term electricity sales price while minimizing the net

power fluctuation penalties. The multi-period EAR problem is formulated as a stochastic MIQP problem with time-coupling constraints on the average number of switching actions. This model uses a direct power evaluation method to analytically express the PV power output of each EAR strategy. Moreover, a switching matrix is designed to simplify the calculation of the number of switching actions.

2) A novel solution method is proposed to address challenges including the combinatorial explosion of EAR strategies, the unpredictability of irradiance distribution, and time-coupling constraints involving state transitions. The proposed method constructs a reduced set of EAR strategies and develops a Lyapunov optimization-based online algorithm to decouple the time-coupling constraints. As a result, the original multi-period EAR method is transformed into a deterministic single-period problem driven by real-time observable information, which ensures that EAR strategies can be solved online while maintaining the average number of switching actions within the specified upper limit.

3) Numerical experiments show that the net power fluctuation penalty of the proposed method is the lowest, at 22% and 50% of that of the non-reconfiguration and traditional power maximization methods, respectively. The total revenue of the proposed method exceeds that of the non-reconfiguration method by 61.0%. Furthermore, the scalability of the proposed method to larger PV arrays has been validated, demonstrating consistent performance improvements.

The rest of this paper is organized as follows. Section II presents system models. Section III details the solution of the proposed model. Section IV presents case studies to test the performance of the proposed method. Finally, the conclusion and future works are given in Section V.

II. System Models

We consider a distribution network with high penetration of PV systems. The PV array reconfiguration is performed in a discrete-time manner with a time interval Δt. The time slots are indexed by t in $\mathcal{T}:=\{1,2,\dots,T\}$. The distribution network with high penetration of PV systems is shown in Fig. 1.

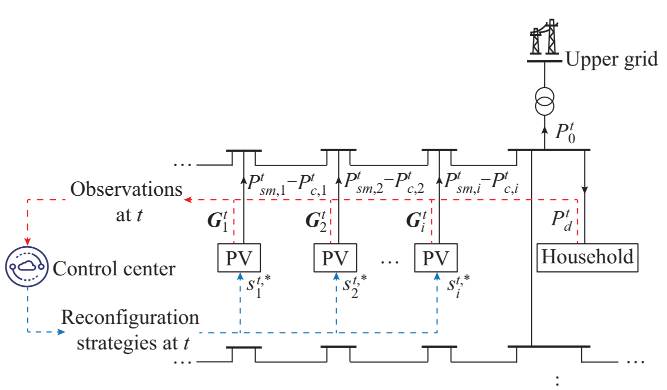

Fig. 1. Distribution network with high penetration of PV systems.

$\boldsymbol{S}_i^{t,*}$ of PV i at time slot t is calculated using $\boldsymbol{G}_i^t$ and P_d^t. Notably, energy storages are not considered in the distribution network for two reasons: ① many residential PV systems lack energy storages due to their high cost; and ② excluding energy storage highlights the performance of the proposed method for grid operations.

A. Problem Formulation

Consider a distributed PV system with multi-PV arrays and an integrated load (the aggregated power demand at the point of common coupling). Let $\mathcal{I}:=\{1,2,\dots,I\}$ be the set of all PV arrays in the system. Each PV array $i\in\mathcal{I}$ has a total-cross-tied (TCT)-structure with M_i rows and N_i columns, and $\mathcal{M}_i:=\{1,2,\dots,M_i\}$ and $\mathcal{N}_i:=\{1,2,\dots,N_i\}$ are the sets of rows and columns, respectively. The set of all modules in PV array i is denoted by $\mathcal{J}_i:=\{1,2,\dots,J_i\}$, where $J_i=M_i\times N_i$. Let $\mathcal{A}_i:=\{1,2,\dots,A_i\}$ collect all the EAR strategies of PV i. Let $\boldsymbol{S}_{i,a_i}^t\in\mathbb{R}^{J_i\times 1}$ be the $a_i\in\mathcal{A}_i$ EAR strategy of PV $i\in\mathcal{I}$ at time slot t. The element of $\boldsymbol{S}_{i,a_i}^t$, i.e., S_{i,a_i,j_i}^t, is the electrical position of the module located at physical location j_i. Let $\boldsymbol{u}_i^t\in\mathbb{B}^{A_i\times 1}$ be an indicator of the EAR strategy $\boldsymbol{S}_{i,a_i}^t$. The element of $\boldsymbol{u}_i^t$, i.e., u_{i,a_i}^t, is a 0-1 variable. If u_{i,a_i}^t is equal to 1, the corresponding $\boldsymbol{S}_{i,a_i}^t$ is selected. The decision variables of the economic operation optimization model are $\boldsymbol{u}_i^t$ and $P_{c,i}^t$.

Let $\boldsymbol{z}_i^t:=[[\boldsymbol{u}_i^t]^{\mathrm{T}}, P_{c,i}^t]^{\mathrm{T}}$ collect all the decision variables of PV i at time slot t. The multi-period EAR problem $\mathbb{P}_1$ can be formulated as:

$$\max_{\{\{\boldsymbol{z}_i^t\}_{i=1}^I\}_{t=1}^T}\ \lim_{T\to\infty}\frac{1}{T}\left[\sum_{t=1}^T \pi^t\Delta t P_0^t-\alpha\left(\frac{P_0^t-P_0^{t-1}}{\sum_{i=1}^I P_{PV,i}}\right)^2\right] \tag{1a}$$

$$P_0^t=\sum_{i=1}^I\left(P_{sm,i}^t-P_{c,i}^t\right)-P_d^t\quad \forall t \tag{1b}$$

$$0\le P_{c,i}^t\le P_{sm,i}^t\quad \forall t,\forall i \tag{1c}$$

$$P_{sm,i}^t=f\left(\boldsymbol{S}_i^{t,*},\boldsymbol{G}_i^t\right)\quad \forall t,\forall i \tag{1d}$$

$$\boldsymbol{S}_i^{t,*}=\sum_{a_i=1}^{A_i}u_{i,a_i}^t\boldsymbol{S}_{i,a_i}^t\quad \forall t,\forall i \tag{1e}$$

$$\boldsymbol{S}_{i,a_i}^t\in\boldsymbol{S}_i^t\quad \forall t,\forall i \tag{1f}$$

$$\sum_{a_i=1}^{A_i}u_{i,a_i}^t=1\quad \forall t,\forall i \tag{1g}$$

$$u_{i,a_i}^t\in\{0,1\}\quad \forall t,\forall i \tag{1h}$$

$$\lim_{T\to\infty}\frac{1}{T}\sum_{t=1}^T\mathbb{E}\left[q\left(\boldsymbol{S}_i^{t,*},\boldsymbol{S}_i^{t-1,*}\right)\right]\le Q\quad \forall i \tag{1i}$$

where $q(\boldsymbol{S}_i^{t,*},\boldsymbol{S}_i^{t-1,*})$ is the number of switching actions required for PV i to switch from $\boldsymbol{S}_i^{t-1,*}$ to $\boldsymbol{S}_i^{t,*}$.

The objective function of $\mathbb{P}_1$ is the expectation of the summarized total revenue of all PV arrays at time slot t. The objective function consists of two components: ① π^t and P_0^t; and ② penalty for net power fluctuations. A quadratic function with coefficient α is designed to penalize the fluctuation of net power between two time slots. Let $\boldsymbol{\Theta}^t:=\{P_d^t,\{\boldsymbol{G}_i^t\}_{i=1}^I\}_{t=1}^T$ collect all random variables in (1). The realization of G^t_{i,m_i,n_i} is unknown in $\mathbb{P}_1$ since $\mathbb{P}_1$ is formulated and solved from a long-term view. Thus, the expectation is taken over the vector $\boldsymbol{\Theta}^t, \forall t$.

Constraint (1b) indicates the difference of the actual PV power output and the load. Constraint (1c) confines the curtailment of PVs to a reasonable range. Constraint (1d) indicates the relationship of the maximum power output with $\boldsymbol{S}_i^{t,*}$ and $\boldsymbol{G}_i^t$ of PV i at time slot t. Constraints (1e) to (1h) ensure that only one of the A_i EAR strategies is selected at each time slot t. Constraint (1i) limits the average number of switching actions within Q.

B. Analytical Expression of Maximum PV Power Output

In this subsection, we establish the analytical expression for the maximum PV power output of a TCT-structured PV array in $\mathbb{P}_1$, i.e., $f(\boldsymbol{S}_i^{t,*}, \boldsymbol{G}_i^t)$. The TCT structure is selected to not only achieve the lowest mismatch loss, but also provide the highest reliability.

G^t_{r,i,m_i} is expressed as [33]:

$$G^t_{r,i,m_i} = \sum_{n_i=1}^{N_i} G^t_{i,m_i,n_i} \quad m_i = 1,2,\ldots,M_i, \forall t, \forall i \tag{2}$$

I^t_{r,i,m_i} is proportional to the sum of the irradiance values of all modules in that row [33]:

$$I^t_{r,i,m_i} = \frac{G^t_{r,i,m_i}}{G_0} I_{m,i} \quad m_i = 1,2,\ldots,M_i, \forall t, \forall i \tag{3}$$

Since the current flowing through the entire PV array is the same at any given time, due to PSCs, rows that cannot achieve higher current values are bypassed by diodes to protect them from damage. Assuming there are s different total irradiances on the modules in rows of PV i at time slot t, arranged in descending order [33] as:

$$G^t_{r,i,1} > G^t_{r,i,2} > \ldots > G^t_{r,i,w_i} > \ldots > G^t_{r,i,W_i} \quad w_i = 1,2\ldots,W_i, \forall t, \forall i \tag{4}$$

The number of rows with G^t_{r,i,w_i} is represented by m^t_{r,i,w_i} and satisfies the following relationship [33]:

$$\sum_{w_i=1}^{W_i} m^t_{r,i,w_i} = M_i \quad \forall t, \forall i \tag{5}$$

If any row of the PV array is bypassed, the output voltage drops to a lower level, resulting in multiple power peaks in the P-V curve. The voltage, current, and power at each power peak of the TCT-structured PV array can be approximated by [33]:

$$V^t_{m,i,w_i} = \left(\sum_{x_i=1}^{w_i} m^t_{r,i,w_i}\right) V_{m,i} \quad \forall t, \forall i \tag{6}$$

$$I^t_{m,i,w_i} = \frac{G^t_{r,i,w_i}}{G_0} I_{m,i} \quad \forall t, \forall i \tag{7}$$

$$P^t_{m,i,w_i} = V^t_{m,i,w_i} I^t_{m,i,w_i} = \left(\sum_{x_i=1}^{w_i} m^t_{r,i,w_i}\right) \frac{G^t_{r,i,w_i}}{G_0} V_{m,i} I_{m,i} \quad \forall t, \forall i \tag{8}$$

Thus, the maximum PV power output of the PV array can be obtained as:

$$P^t_{sm,i} = \max\left(P^t_{m,i,w_i}\right) \quad w_i = 1,2,\ldots,W_i, \forall t, \forall i \tag{9}$$

C. Counting Model of PV Switching Actions

In this part, we formulate the function that calculates the number of PV switching actions in $\mathbb{P}_1$, i. e., $q(\boldsymbol{S}_i^{t,*}, \boldsymbol{S}_i^{t-1,*})$. The designed switching matrix integrates multiple multi-throw switches, which connect the PV modules to the electrical bus. An example of a 3×3 TCT-structured PV array is shown in Fig. 2 [36]. The colored lines illustrate the correspondence between the PV array connections in Fig. 2(a) and (b).

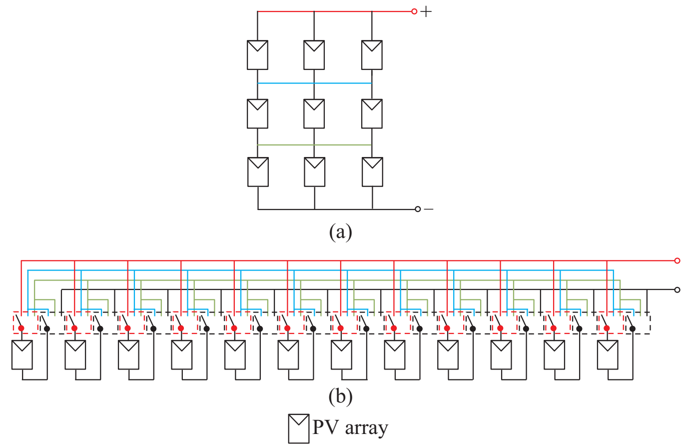

Fig. 2. Example of a 3×3 TCT-structured PV array. (a) 3×3 TCT-structured PV array. (b) Designed switching matrix.

Given the designed switching matrix, each PV module can be equally connected to any row. Each change in the position of a PV module is counted as one switching action. Thus, the number of switching actions is determined by the difference between $\boldsymbol{S}_i^{t-1,*}$ and $\boldsymbol{S}_i^{t,*}$ as:

$$q(\boldsymbol{S}_i^{t,*}, \boldsymbol{S}_i^{t-1,*}) = \sum_{j_i=1}^{J_i} \delta(\boldsymbol{S}_i^{t,*}, \boldsymbol{S}_i^{t-1,*}) \quad \forall t, \forall i \tag{10}$$

$$\delta(\boldsymbol{S}_i^{t,*}, \boldsymbol{S}_i^{t-1,*}) = \begin{cases} 1 & S^{t,*}_{i,j} \neq S^{t-1,*}_{i,j}, \forall t, \forall i \\ 0 & S^{t,*}_{i,j} = S^{t-1,*}_{i,j}, \forall t, \forall i \end{cases} \tag{11}$$

where $\delta(\boldsymbol{S}_i^{t,*}, \boldsymbol{S}_i^{t-1,*})$ is an indicator.

Remark 1

Existing research works have proposed several PV array structures, including series, parallel, series-parallel, TCT, bridged-linked, honey-comb, etc. In $\mathbb{P}_1$, the structure of PV arrays is related to the analytical expression of the maximum PV power output and counting model of the switching actions. By carefully designing them, the multi-period EAR model can be established for PV array of other structures.

III. Solution Method

It is challenging to solve the multi-period EAR model for the following reasons.

1) For an $M_i \times N_i$ PV array, there are $(M_i \times N_i)!$ EAR strategies at each time slot. As the number of PV modules increases, the number of EAR strategies grows exponentially, leading to a combinatorial explosion and making the computation infeasible.

2) It is difficult to predict or probabilistically characterize $\boldsymbol{G}_i^t$ on a PV array. Consequently, traditional methods that re-

ly on the predict information of random variables are ineffective for solving the multi-period EAR model.

3) The time-coupling constraints in (1i) involve state transitions that exhibit Markov properties. The dependencies between the state transitions at different time slots make traditional methods such as static optimization or standard dynamic programming unsuitable for solving this model.

To address these challenges, we introduce a rule-driven method to construct a reduced set of EAR strategies to address the combinatorial explosion problem. Then, the Lyapunov optimization-based online algorithm is used to transform the multi-period stochastic optimization problem into a single-period deterministic problem. Thereby, the EAR strategies can be computed using observable information.

A. Construction of a Reduced Set of EAR strategies

1) Rule 1: this rule is excluding EAR strategies that result in a lower PV power output than that of the current PV topology:

$$\tilde{\boldsymbol{S}}_i^t=\{\boldsymbol{S}_{i,a}^t|f(\boldsymbol{S}_{i,a}^t,\boldsymbol{G}_i^t)>f(\boldsymbol{S}_i^{t-1,*},\boldsymbol{G}_i^t),\boldsymbol{S}_{i,a}^t\in\boldsymbol{S}_i^t\}\quad\forall t,\forall i \tag{12}$$

2) Rule 2: this rule is excluding EAR strategies that require more switching actions to achieve the same PV power output:

$$\tilde{\boldsymbol{S}}_i^t=\{\boldsymbol{S}_{i,a}^t|\min q(\boldsymbol{S}_{i,a}^t,\boldsymbol{S}_i^{t-1,*}),\boldsymbol{S}_{i,a}^t\in\boldsymbol{S}_i^t\}\quad\forall t,\forall i \tag{13}$$

These rules ensure that $\boldsymbol{S}_i^t$ only contains necessary EAR strategies, thus improving the computational efficiency.

Remark 2

For large-scale PV arrays, obtaining a set of EAR strategies is impractical due to the vast number of PV modules. In this case, we can divide the PV modules into sub-arrays or design the array as a partially reconfigurable arrays [27], [28].

B. Handling of Time-coupling Constraint

To decouple the time-coupling constraints in (1i), the technique of virtual queues [37]-[39] is leveraged to reformulate $\mathbb{P}_1$. H_i^t is defined for all $i\in\mathcal{I}$ as:

$$H_i^{t+1}=H_i^t+\eta\max[q(\boldsymbol{S}_i^{t,*},\boldsymbol{S}_i^{t-1,*})-Q,0]\quad\forall i,\forall t \tag{14}$$

The arrival rate of the queue is the input switching action while the departure rate is the switching action per unit time Q at time slot t. η is the queue-update step size, which represents the sensitivity of the virtual queue to switching violations. A larger η means the virtual queue responds more strongly to excessive switching actions exceeding limit Q, leading to stricter enforcement of constraints but potentially reducing total revenue. Conversely, a smaller η makes the queue less sensitive to switching violations, providing more flexibility in switching actions but risking violation of long-term switching constraints.

Following the rate stability theorem [37], we place (1i) with:

$$\lim_{T\to\infty}\frac{\sum_{t=1}^{T}\mathbb{E}(H_i^t)}{T}=0\quad\forall i \tag{15}$$

The constraint (14) still hinders the online deployment as it is coupled over a long-term horizon. Consequently, the Lyapunov optimization-based online algorithm is used to transfer them to a penalty term attached to the objective function at each time slot based on the observation of the current states.

Let $\boldsymbol{H}^t\in\mathbb{R}^{I\times 1}$ collect all the virtual queues of PV $i\in I$. Then, we define a Lyapunov function $\left\|\frac{1}{2}\boldsymbol{H}^t\right\|^2$ to measure the size of the queues. Then, the conditional one-slot Lyapunov drift can be defined as follows to measure the expected queue size growth under observation of current state $\boldsymbol{H}^t$:

$$\Delta L(\boldsymbol{H}^t)=\mathbb{E}\left[\frac{1}{2}\left(\|\boldsymbol{H}^{t+1}\|^2-\|\boldsymbol{H}^t\|^2\right)\right] \tag{16}$$

To ensure the stability of the queues, it is necessary to choose an EAR strategy that minimizes the value of $\Delta L(\boldsymbol{H}^t)$, i.e., the virtual queues are kept uncrowded. Simultaneously, the original objective function of $\mathbb{P}_1$ should be considered, which is to improve revenue from electricity sales and reduce penalties of net power fluctuations. To achieve this, $\mathbb{P}_1$ can be transformed into maximizing F^t at time slot using the drift-plus-penalty method [37]:

$$F^t=F_1^t-\Delta L(\boldsymbol{H}^t)\quad\forall t \tag{17}$$

where $F_1^t=\pi^t\Delta tP_0^t-\alpha\left[(P_0^t-P_0^{t-1})\Big/\sum_{i=1}^{I}P_{PV,i}\right]^2$ is the initial optimization objective of $\mathbb{P}_1$ at each time slot.

Furthermore, (16) has an upper bound, thus the solution process can be simplified as:

$$F^t=F_1^t-\Delta L(\boldsymbol{H}^t)\le-\frac{\eta N}{2}(\max[N-Q,0])^2+F_1^t-\sum_{i=1}^{N}\eta H_i^t\max[q(S_i^t,S_i^{t-1})-Q,0] \tag{18}$$

Since $-\frac{\eta N}{2}(\max[N-Q,0])^2+F_1^t$ is a constant, it is only necessary to find the maximum value of $F^t=F_1^t+F_2^t$.

$$F_2^t=-\sum_{i=1}^{N}\eta H_i^t\max[q(\boldsymbol{S}_i^{t,*},\boldsymbol{S}_i^{t-1,*})-Q,0]\quad\forall t \tag{19}$$

C. Time-decoupled Reformulation

Based on the processes introduced in Sections III-A and III-B, the original $\mathbb{P}_1$ is reformulated as a new problem $\mathbb{P}_2^t,\forall t$, given by:

$$\max_{\{z_i^t\}_{i=1}^I}\pi^t\Delta tP_0^t-\alpha\left[(P_0^t-P_0^{t-1})\Big/\sum_{i=1}^{I}P_{PV,i}\right]^2-\sum_{i=1}^{N}\eta H_i^t\max[q(\boldsymbol{S}_i^{t,*},\boldsymbol{S}_i^{t-1,*})-Q,0] \tag{20a}$$

$$\text{(1b)-(1d)} \tag{20b}$$

$$\boldsymbol{S}_i^{t,*}=\sum_{a_i=1}^{\tilde{A}_i^t}u_{i,a_i}^t\boldsymbol{S}_{i,a_i}^t\quad\forall i \tag{20c}$$

$$\boldsymbol{S}_{i,a_i}^t\in\tilde{\boldsymbol{S}}_i^t\quad\forall i \tag{20d}$$

$$\sum_{a_i=1}^{\tilde{A}_i^t}u_{i,a_i}^t=1\quad\forall i \tag{20e}$$

$$u_{i,a_i}^t\in\{0,1\}\quad\forall i \tag{20f}$$

It is worth noting that the above transformation process is not entirely rigorous. The main source of error comes from the size of the upper bound gap. In simple terms, reducing η can narrow the gap produced by the relaxation but also simultaneously reduces the weight of F_2^t in the objective function. The correct choice of η can improve the closeness of the solution to the theoretically optimal solution while ensuring that the constraint of (1i) is satisfied.

Hereafter, $\mathbb{P}_1$ comprising the time-coupling constraints is reformulated as a single-period deterministic problem to be executed at each time slot without reliance on high-complex solvers.

Remark 3

$\mathbb{P}_2$ is an MIQP problem that can be efficiently solved using commercial solvers. It can also be solved using distributed optimization algorithms [39], [40].

Furthermore, a flowchart of the proposed method is outlined in Fig. 3.

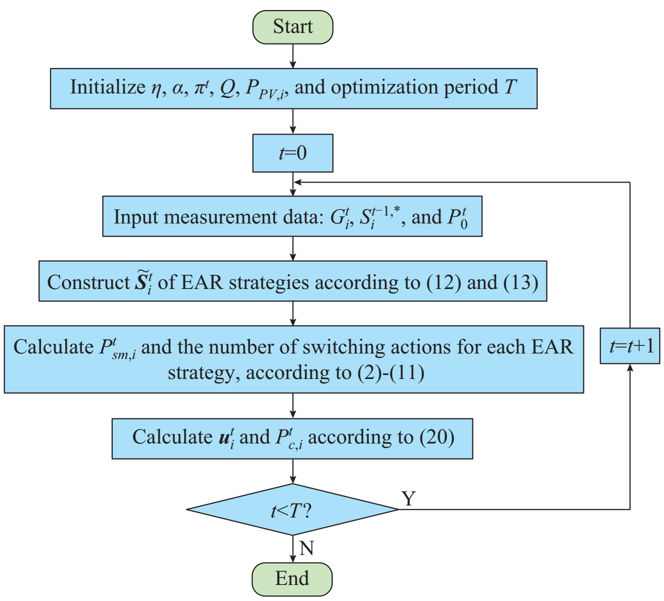

Fig. 3. Flowchart of proposed method.

IV. Result and Discussion

A residential PV system with two rooftop TCT-structured PV arrays and an integrated load is used to verify the proposed method. Each PV array consists of three PV strings, where each string consists of four JinkoSolar JKM630N-78HL4-V PV modules connected in series. Table I shows the PV module specification. The entire optimization period is 1 hour, while it is divided into 60 time slots. During the entire optimization period, the irradiance on the unshaded PV modules changes from 780 W/m^2 to 1000 W/m^2 in increments of 20 W/m^2 every 6 min. Severely shaded modules receive an irradiance of 400 W/m^2, while slightly shaded modules receive 700 W/m^2. Different PSCs are considered on the two PV arrays. PSCs on PV1 include: ① one module with slight shading; ② three modules with slight shading; and ③ three modules with slight shading plus three modules with severe shading. PSCs on PV2 include: ① one module with slight shading; ② two modules with slight shading; and ③ three modules with slight shading plus two modules with severe shading. The normal condition and PSCs occur randomly throughout the optimization period, and the location of the shaded modules is also random. The upper bound for the average number of switching actions per unit time is set to be 1.2. The load varies between 4.90 kW and 5.81 kW with a time resolution of 1 min. The fluctuation penalty coefficient is 0.0005, the electricity sales price is 0.773 CNY/kWh, and $\eta=60$. Simulations are run in MATLAB R2022a with the Gurobi solver.

TABLE I
PV Module Specification

Parameter	Value
Peak power (W)	630.00
Rated current (A)	46.02
Rated voltage (V)	13.69

A. Comparison with Existing Methods

In this subsection, we compare the performance of the proposed method with existing methods in terms of the maximum PV power output, the actual PV power output, the net power fluctuation, and the total revenue. The benchmarks include the conventional power maximization method [15]-[27], aiming to maximize the PV power output at each time slot and the non-reconfiguration method.

1) The Maximum PV Power Output

Figure 4 shows the maximum PV power output using different methods. It can be observed that the maximum PV power output reconfigured using the proposed method is always higher than that of the non-reconfiguration method. However, sometimes the maximum PV power output reconfigured using the proposed method is lower than that of the conventional power maximization method. This shows that maximizing the PV power output does not always align with the operation requirements of net power smoothing.

Furthermore, Fig. 5 shows the number of switching ac-

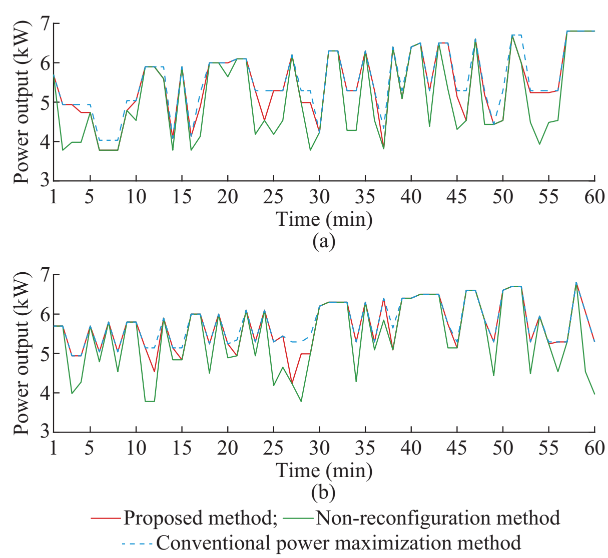

Fig. 4. The maximum PV power output using different methods. (a) PV1. (b) PV2.

tions of PV1 using the proposed method and the conventional power maximization method. As shown in Fig. 4(a), the proposed method achieves near-maximum PV power output with minimal or zero switch actions at the 3rd to 10th and the 51st to 56th min. Conversely, the proposed method increases switching actions above the upper limit at the 33rd, 34th, 42nd, and 44th min to prevent the low PV power output observed in the non-reconfiguration method. This demonstrates that the proposed method effectively allocates switching resources throughout the optimization period.

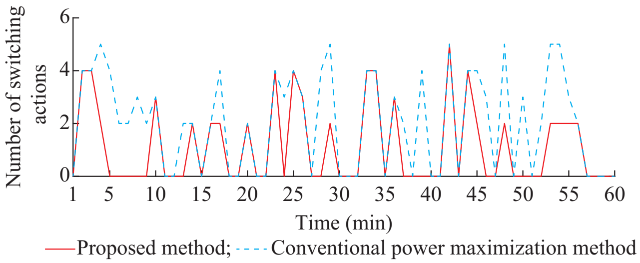

Fig. 5. Number of switching actions of PV1 using proposed method and conventional power maximization method.

In Fig. 6, the topology of PV2, the irradiance of each module, and sum of irradiance of modules in each row at the 27th and 28th min are presented. PV2 has the greatest variation in irradiance between rows using the non-reconfiguration method, resulting in the most uneven irradiance of modules. In contrast, the proposed method improves the uniformity of the sum of irradiance of modules between rows compared with the non-reconfiguration method. PV2 reconfigured using the conventional power maximization method has the most uniform irradiance of modules across its rows. Consequently, at the 28th min, PV2 reconfigured using the conventional power maximization method achieves the highest peak power output, followed by the proposed method, while the non-reconfigured method has the lowest peak power output. These results are consistent with those in Fig. 4(b).

2) Actual PV Power Output

Figure 7 shows the actual power output and curtailment of PV1 and PV2. The actual PV power output is usually equal to the maximum PV power output, indicating that the PV arrays are primarily reconfigured to obtain the optimal power output. However, at some minutes, the PV generation is curtailed to ensure the stability of the actual PV power output or to comply with the limits of the switch actions.

Table II further summarizes the maximum PV power output and actual PV power output using the three methods. It can be observed that both the proposed method and the conventional power maximization method increase the maximum PV power output compared with the non-reconfiguration method. Furthermore, the maximum PV power output of the proposed method is lower than the actual PV power output due to the consideration of smoothing the net power fluctuations. Even in this case, the total actual power output of two PV arrays remains 3.7% higher than that of the non-reconfiguration method.

Fig. 6. Topology of PV2, irradiance of each module, and sum of irradiance of modules in each row at the 27th and 28th min. (a) Non-reconfiguration method. (b) Proposed method. (c) Conventional power maximization method.

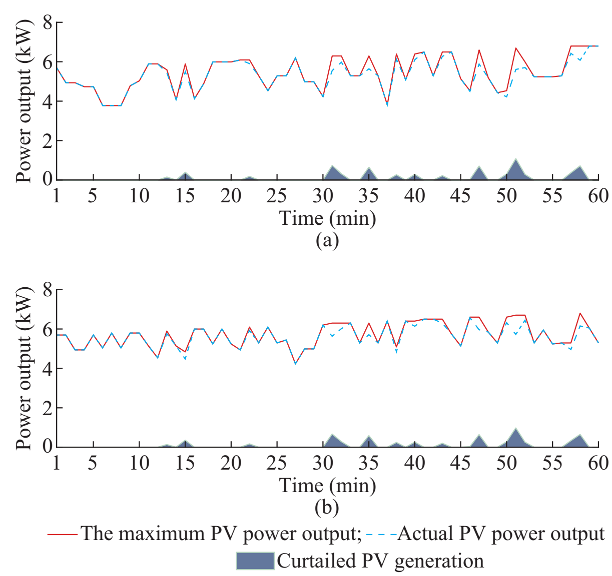

Fig. 7. Actual power output and curtailment of PV1 and PV2. (a) PV1. (b) PV2.

3) Net Power Fluctuation

Figure 8 illustrates the net power fluctuation curve using different methods. It can be observed that the net power of the proposed method consistently lies between the net power curves of the conventional power maximization method and the non-reconfiguration method. The proposed method exhibits smaller power fluctuations compared with the benchmarks. The fluctuation penalties of the proposed method, the conventional power maximization method, and the non-reconfiguration method are 0.35 CNY, 0.70 CNY, and 1.59 CNY, respectively, which indicate that the fluctuation penalty of the proposed method is the lowest (at 50% of the conventional power maximization method and 22% of the non-reconfiguration method). The difference compared with the unconstrained switching method indicates the impact of PV power output fluctuations on the net power. This finding highlights the importance of considering grid operation requirements rather than solely focusing on maximizing PV power output.

TABLE II
THE MAXIMUM PV POWER OUTPUT AND ACTUAL PV POWER OUTPUT OF THREE METHODS

Method	The maximum PV power output (kWh)		Actual power PV output (kWh)	
	PV1	PV2	PV1	PV2
Proposed method	5.44	5.70	5.33	5.60
Non-reconfiguration method	5.12	5.42	5.12	5.42
Conventional power maximization method	5.55	5.77	5.55	5.77

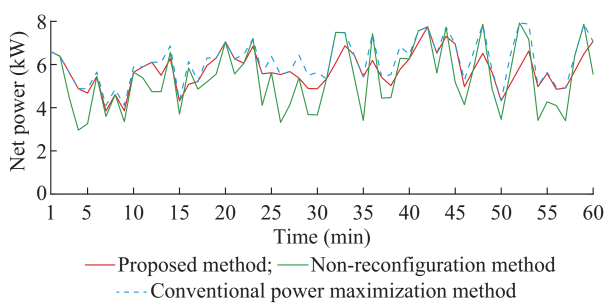

Fig. 8. Net power fluctuation curve using three methods.

4) Total Revenue

Table III compares the total revenue among different methods. The proposed method generates the highest total revenue, closely followed by the conventional power maximization method. The non-reconfiguration method generates the lowest revenue, which is 61.0% lower than the proposed method.

TABLE III
TOTAL REVENUE AMONG DIFFERENT METHODS

Method	Electricity sales price (CNY)	Net power fluctuation penalty (CNY)	Total revenue (CNY)
Proposed method	4.44	0.35	4.09
Non-reconfiguration method	4.13	1.59	2.54
Conventional power maximization method	4.74	0.70	4.04

B. Impact of Different Factors

In this subsection, we analyze the impact of different factors considered in the proposed method, including the net power fluctuation penalty, the constraints on the average number of switching actions, and the queue-update step size.

1) Net Power Fluctuation Penalty

Figure 9 illustrates the net power fluctuation curves for the proposed method with and without considering net power fluctuation. The fluctuation penalty of the benchmark is 0.93 CNY, which is 2.65 times that of the proposed method. These results demonstrate the necessity of considering the net power fluctuation penalty.

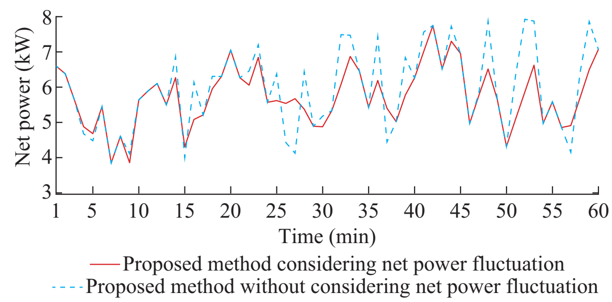

Fig. 9. Net power fluctuation curves for proposed method with and without considering net power fluctuation.

2) Constraints on Average Number of Switching Actions

Figure 10 shows the average number of switching actions of PV1 and PV2 for the proposed method with and without considering the average switching action constraint. It can be observed that the proposed method reduces the average number of switching actions below the upper bound as the operation time increases. These results demonstrate the effectiveness of the method outlined in Section III-B.

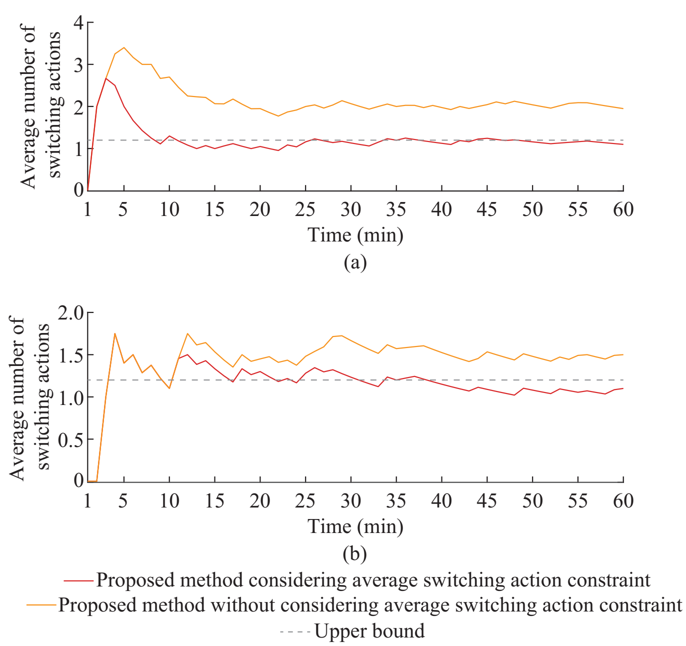

Fig. 10. Average number of switching actions of PV1 and PV2 for proposed method with and without considering average switching action constraint. (a) PV1. (b) PV2.

3) *Queue-update Step Size*

Figure 11 illustrates the variation of total revenue and the number of switch actions with queue-update step size. When $\eta=0$, equivalent to an unconstrained switching method, both the number of switching actions and total revenue reach their maximum values. As η increases, the number of switching actions and the total revenue decreases, showing that the choice of η is crucial to ensure that the number of switching actions meets the requirements while achieving high total revenue.

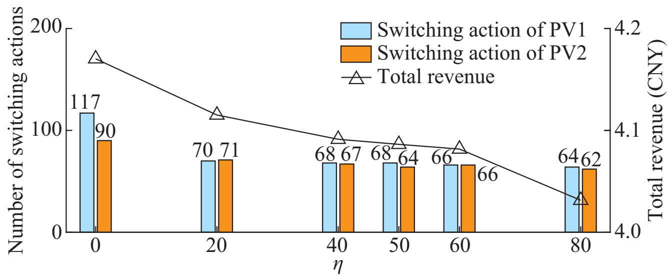

Fig. 11. Variation of total revenue and number of switch actions with queue-update step size.

4) *Fluctuation Penalty Coefficients*

Figure 12 illustrates the total revenue under different α. We use a logarithmic scale to represent the wide range of α. It can be observed that the non-reconfiguration method always has the lowest total revenue. When $\alpha=10^{-4}$ (the fluctuation penalty effect becomes negligible), the objective of the proposed method becomes close to that of the conventional power maximization method. Due to the limited number of switching actions, the total revenue of the proposed method is slightly lower than that of the conventional power maximization method. When α increases from 0.0001 to 0.1, the total revenues of all methods decrease due to the fluctuation penalty. In this case, the proposed method shows better performance than benchmarks, with its advantage growing until α becomes extremely large ($\alpha=0.1$). These results demonstrate that the proposed method has the highest total revenue in most cases.

C. *Scalability to Larger PV System*

A 9×12 TCT-structured PV system is used for testing the proposed method. The PV array consists of 108 PV modules (specifications are shown in Table I) with an array capacity of 68.04 kW. We divide modules into sub-arrays. The size of the divided sub-array is determined as 3×4. The entire optimization period is 1 hour, divided into 60 sub-periods, with optimization calculations performed every minute. Throughout the entire optimization period, the irradiance on the unshaded PV modules in both PV arrays changes from 780 W/m^2 to 1000 W/m^2 in increments of 20 W/m^2 every 6 min. Severely shaded modules receive an irradiance of 400 W/m^2, while slightly shaded modules receive 700 W/m^2. Different PSCs are considered for the PV array. There are four PSCs: ① one module with slight shading; ② three modules with slight shading plus five modules with severe shading; ③ five modules with slight shading plus three modules with severe shading; and ④ four modules with slight shading plus five modules with severe shading. The normal condition and PSCs occur randomly throughout the optimization period, and the location of the shaded modules is also random. The load varies between 19.66 kW and 23.24 kW, with a time resolution of 1 min. The upper bound for the average number of switching actions per unit time, the net power fluctuation penalty, the electricity sales price, and the virtual queue-update step size are the same as before. Results are presented in Table IV, which verify that the proposed method effectively reduces net power fluctuation penalty, reducing the penalty by 74.2% compared with that of the non-reconfiguration method and by 60.8% compared with that of the conventional power maximization method. The proposed method achieves the highest total revenue, approximately 6.4 times that of the non-reconfiguration method and 42.9% higher than that of the conventional power maximization method. These results validate the scalability of the proposed method to larger PV system.

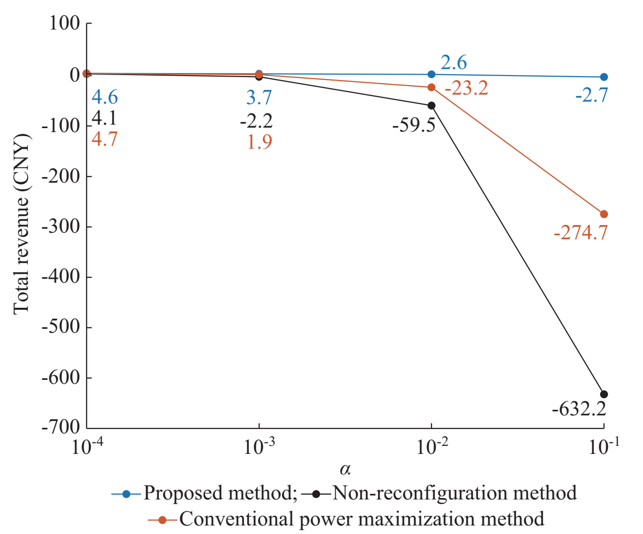

Fig. 12. Total revenue under different α.

TABLE IV
RESULTS OF A LARGER PV SYSTEM

Method	The maximum PV power output (kWh)	Actual PV power output (kWh)	Net power fluctuation penalty (CNY)	Electricity sales price (CNY)	Total revenue (CNY)
Proposed method	45.6	44.51	3.88	18.37	14.49
Non-reconfiguration method	43.09	43.09	15.03	17.28	2.25
Conventional power maximization method	46.67	46.67	9.9	20.04	10.14

V. Conclusion

This paper proposes a multi-period EAR method for multi-PV systems considering net power fluctuation mitigation, maximizing revenue by balancing electricity sales price and net power fluctuation penalties. The EAR problem is formulated as a stochastic MIQP problem with time-coupling constraints on the average number of switching actions. To handle the unpredictability of PSCs, a Lyapunov optimization-based online algorithm is proposed to decouple the time-coupling constraints involving state transitions. As a result, the original model is transformed into a single-period deterministic problem, allowing for the rapid development of EAR strategies based on observable information during each period.

The proposed method is first validated in residential PV systems. Simulation results show that the proposed method has the lowest net power fluctuation penalty, which is 50% of the conventional power maximization method and 22% of the non-reconfiguration method. The total revenue of the proposed method is 61% higher than that of the non-reconfiguration method. The average number of switch actions over the entire period does not exceed the predetermined upper bound. We further verify the effectiveness of the proposed method on a larger PV array.

Future work can consider more specific operation requirements of different grids, the impact of distributed PV locations, and the co-optimization with energy storage systems to further enhance the practical applicability of the proposed method.

References

[1] M. Wang, X. Xu, Z. Yan *et al*., "An online optimization method for extracting parameters of multi-parameter PV module model based on adaptive Levenberg-Marquardt algorithm," *Energy Conversion and Management*, vol. 245, p. 114611, Oct. 2021.

[2] K. Wang, J. Ma , X. Lu *et al*., "Virtual reality based shading pattern recognition and interactive global maximum power point tracking in photovoltaic systems," *Journal of Modern Power Systems and Clean Energy*, vol. 12, no. 6, pp. 1849-1858, May 2024.

[3] C. Wang, M. Li, Y. Cao *et al*., "Gradient boosting dendritic network for ultra-short-term PV power prediction," *Frontiers in Energy*, vol. 18, pp. 785-798, Jan. 2024.

[4] M. Wang, X. Xu, and Z. Yan, "Online fault diagnosis of PV array considering label errors based on distributionally robust logistic regression," *Renewable Energy*, vol. 203, pp. 68-80, Feb. 2023.

[5] Z. Tan, Z. Yan, H. Zhong *et al*., "Non-iterative solution for coordinated optimal dispatch via equivalent projection – part I: theory," *IEEE Transactions on Power Systems*, vol. 39, no. 1, pp. 890-898, Mar. 2024.

[6] L. Li, S. Fan, J. Xiao *et al*., "Fair trading strategy in multi-energy systems considering design optimization and demand response based on consumer psychology," *Energy*, vol. 306, p. 132393, Oct. 2024.

[7] Y. Li, Y. Ding, S. He *et al*., "Artificial intelligence-based methods for renewable power system operation," *Nature Reviews Electrical Engineering*, vol. 1, pp. 163-179, Mar. 2024.

[8] X. Zhang and M. Wang, "Optimal photovoltaic array reconfiguration for alleviating the partial shading influence based on particle swarm optimization," in *Proceedings of 2022 IEEE 6th Conference on Energy Internet and Energy System Integration*, Chengdu, China, Oct. 2022, pp. 988-993.

[9] D. Ahluwalia, S. Anjum, and V. Mukherjee, "Boost in energy generation using robust reconfiguration: a novel scheme for photovoltaic array under realistic fractional partial shadings," *Energy Conversion and Management*, vol. 290, p. 117211, Aug. 2023.

[10] G. S. Krishna and T. Moger, "Reconfiguration strategies for reducing partial shading effects in photovoltaic arrays: state of the art," *Solar Energy*, vol. 182, pp. 429-452, Apr. 2019.

[11] L. Manna, V. L. Vigni, E. R. Sanseverino *et al*., "Reconfigurable electrical interconnection strategies for photovoltaic arrays: a review," *Renewable and Sustainable Energy Reviews*, vol. 33, pp. 412-426, May 2014.

[12] S. Rezazadeh, A. Moradzadeh, K. Pourhossein *et al*., "Photovoltaic array reconfiguration under partial shading conditions for maximum power extraction: a state-of-the-art review and new solution method," *Energy Conversion and Management*, vol. 258, p. 115468, Apr. 2022.

[13] G. Velasco-Quesada, F. Guinjoan-Gispert, R. Piqué-López *et al*., "Electrical PV array reconfiguration strategy for energy extraction improvement in grid-connected PV systems," *IEEE Transactions on Industrial Electronics*, vol. 56, no. 11, pp. 4319-4331, Nov. 2009.

[14] P. Aravind, S. Sugumar, and M. Pravin, "Optimal battery based electrical reconfiguration technique for partial shaded PV system," *Applied Energy*, vol. 361, p. 122942, Jan. 2024.

[15] G. Velasco, J. J. Negroni, F. Guinjoan *et al*., "Irradiance equalization method for output power optimization in plant oriented grid-connected PV generators," in *Proceedings of 2005 European Conference on Power Electronics and Applications*, Dresden, Germany, Sept. 2005, pp. 1-10.

[16] J. P. Storey, P. R. Wilson, and D. Bagnall, "Improved optimization strategy for irradiance equalization in dynamic photovoltaic arrays," *IEEE Transactions on Power Electronics*, vol. 28, no. 6, pp. 2946-2956, Jun. 2012.

[17] M. Z. S. El-Dein, M. Kazerani, and M. M. A. Salama, "Optimal photovoltaic array reconfiguration to reduce partial shading losses," *IEEE Transactions on Sustainable Energy*, vol. 4, no. 1, pp. 145-153, Jan. 2012.

[18] A. M. Ajmal, V. K. Ramachandaramurthy, A. Naderipour *et al*., "Comparative analysis of two-step GA-based PV array reconfiguration technique and other reconfiguration techniques," *Energy Conversion and Management*, vol. 230, p. 113806, Feb. 2021.

[19] S. N. Deshkar, S. B. Dhale, J. S. Mukherjee *et al*., "Solar PV array reconfiguration under partial shading conditions for maximum power extraction using genetic algorithm," *Renewable and Sustainable Energy Reviews*, vol. 43, pp. 102-110, Mar. 2015.

[20] T. S. Babu, J. P. Ram, T. Dragičević *et al*., "Particle swarm optimization based solar PV array reconfiguration of the maximum power extraction under partial shading conditions," *IEEE Transactions on Sustainable Energy*, vol. 9, no. 1, pp. 74-85, Jan. 2017.

[21] H. Rezk, A. Fathy, and M. Aly, "A robust photovoltaic array reconfiguration strategy based on coyote optimization algorithm for enhancing the extracted power under partial shadow condition," *Energy Reports*, vol. 7, pp. 109-124, Nov. 2021.

[22] A. Fathy, "Butterfly optimization algorithm-based methodology for enhancing the shaded photovoltaic array extracted power via reconfiguration process," *Energy Conversion and Management*, vol. 220, p. 113115, Sept. 2020.

[23] D. Yousri, S. B. Thanikanti, K. Balasubramanian *et al*., "Multi-objective grey wolf optimizer for optimal design of switching matrix for shaded PV array dynamic reconfiguration," *IEEE Access*, vol. 8, pp. 159931-159946, Aug. 2020.

[24] D. Yousri, T. S. Babu, E. Beshr *et al*., "A robust strategy based on marine predators algorithm for large scale photovoltaic array reconfiguration to smooth the partial shading effect on the performance of PV system," *IEEE Access*, vol. 8, pp. 112407-112426, Jun. 2020.

[25] T. S. Babu, D. Yousri, and K. Balasubramanian, "Photovoltaic array reconfiguration system for maximizing the harvested power using population-based algorithms," *IEEE Access*, vol. 8, pp. 109608-109624, Jun. 2020.

[26] A. Fathy, "Recent meta-heuristic grasshopper optimization algorithm for optimal re-configuration of partially shaded PV array," *Solar Energy*, vol. 171, pp. 638-651, Sept. 2018.

[27] D. Nguyen and B. Lehman, "An adaptive solar photovoltaic array using model-based reconfiguration algorithm," *IEEE Transactions on Industrial Electronics*, vol. 55, no. 7, pp. 2644-2654, Jul. 2008.

[28] K. S. Parlak, "PV array reconfiguration method under partial shading conditions," *International Journal of Electrical Power & Energy Systems*, vol. 63, pp. 713-721, Dec. 2014.

[29] H. Wang, R. Luo, Q. Yu *et al*., "Topology-independent end-to-end learning model for improving the voltage profile in microgrids-integrated power distribution networks," *Frontiers in Energy*, vol. 17, no. 2, pp. 211-227, Dec. 2023.

[30] Y. Zhang, Y. Meng, S. Fan *et al*., "Multi-time scale customer directrix load-based demand response under renewable energy and customer uncertainties," *Applied Energy*, vol. 383, p. 125334, Apr. 2025.

[31] S. Huang, L. Xiong, Y. Zhou *et al*., "Distributed predefined-time control for power system with time delay and input saturation," *IEEE Transactions on Power Systems*, vol. 40, no. 1, pp. 151-165, Jan. 2025.
[32] C. Kirches, *Fast Numerical Methods for Mixed-integer Nonlinear Model-Predictive Control*. Wiesbaden: Vieweg+ Teubner Verlag, 2011.
[33] Z. Zhu, M. Hou, L. Ding *et al*., "Optimal photovoltaic array dynamic reconfiguration strategy based on direct power evaluation," *IEEE Access*, vol. 8, pp. 210267-210276, Nov. 2020.
[34] M. Jazayeri, K. Jazayeri, and S. Uysal, "Adaptive photovoltaic array reconfiguration based on real cloud patterns to smooth effects of nonuniform spatial irradiance profiles," *Solar Energy*, vol. 155, pp. 506-516, Oct. 2017.
[35] E. R. Sanseverino, T. N. Ngoc, M. Cardinale *et al*., "Dynamic programming and Munkres algorithm for optimal photovoltaic arrays reconfiguration," *Solar Energy*, vol. 122, pp. 347-358, Dec. 2015.
[36] X. Zhang, T. Yu, X. Ma *et al*., "An efficient multi-agent negotiation algorithm for multi-period photovoltaic array reconfiguration with a hydrogen energy storage system," *Energy Conversion and Management*, vol. 256, p. 115376, Mar. 2022.
[37] M. J. Neely, "Stochastic network optimization with application to communication and queueing systems," *Synthesis Lectures on Communication Networks*, vol. 3, no. 1, pp. 1-211, Jan. 2010.
[38] W. Shi, N. Li, C. Chu *et al*., "Real-time energy management in microgrids," *IEEE Transactions on Smart Grid*, vol. 8, no. 1, pp. 228-238, Jan. 2017.
[39] S. Fan, G. He, X. Zhou *et al*., "Online optimization for networked distributed energy resources with time-coupling constraints," *IEEE Transactions on Smart Grid*, vol. 12, no. 1, pp. 251-267, Jan. 2020.
[40] Y. Shen, W. Wu, B. Wang *et al*., "Data-driven convexification for frequency nadir constraint of unit commitment," *Journal of Modern Power Systems and Clean Energy*, vol. 11, no. 5, pp. 1711-1717, Sept. 2023.

Mengyuan Wang received the B.S. and M.S. degrees from North China Electric Power University, Beijing, China, in 2016 and 2019, and the Ph.D. degree in electrical engineering from Shanghai Jiao Tong University, Shanghai, China, in 2023, respectively. Since 2023, she has been a Postdoctor of Electrical Engineering with Shanghai Jiao Tong University. Her research interests include machine learning, and operation and maintenance of photovoltaic system.

Xiaoyuan Xu received the B.S. and Ph.D. degrees in electrical engineering from Shanghai Jiao Tong University, Shanghai, China, in 2010 and 2016, respectively. He was a Visiting Scholar with the Robert W. Galvin Center for Electricity Innovation, Illinois Institute of Technology, Chicago, USA, from 2017 to 2018. He is currently an Associate Professor in electrical engineering with Shanghai Jiao Tong University. His research interests include power system uncertainty analysis and optimization.

Shuai Fan received the B.S. degree in electrical engineering from Southwest Jiao Tong University, Chengdu, China, in 2015 and the Ph.D. degree in electrical engineering from Shanghai Jiao Tong University, Shanghai, China, in 2021. He was a Visiting Scholar with Southern Methodist University, Dallas, USA, from 2018 to 2019. He is currently a Research Associate Professor in electrical engineering with Shanghai Jiao Tong University. His research interests include demand response and online optimization in electric power system.

Zheng Yan received the B.S. degree from Shanghai Jiao Tong University, Shanghai, China, in 1984, and the M.S. and Ph.D. degrees from Tsinghua University, Beijing, China, in 1987 and 1991, respectively, all in electrical engineering. He is currently a Professor in electrical engineering with Shanghai Jiao Tong University. His current research interests include application of optimization theory to power system, electricity market, and dynamic security assessment.

Bo Yang received the Ph.D. degree in electrical engineering from the City University of Hong Kong, Hong Kong, China, in 2009. He is currently a Full Professor with Shanghai Jiao Tong University, Shanghai, China. Prior to joining Shanghai Jiao Tong University in 2010, he was a Post-Doctoral Researcher with the KTH Royal Institute of Technology, Stockholm, Sweden, from 2009 to 2010, and a Visiting Scholar with the Polytechnic Institute of New York University, Brooklyn, USA, in 2007. His research interests include optimization and control for energy network and Internet of Things.

Xinping Guan received the B.Sc. degree in mathematics from Harbin Normal University, Harbin, China, in 1986, and the Ph.D. degree in control science and engineering from the Harbin Institute of Technology, Harbin, China, in 1999. He is currently the Chair Professor at Shanghai Jiao Tong University. He is the Leader of the Prestigious Innovative Research Team, National Natural Science Foundation of China. His current research interests include industrial network system, smart manufacturing, and underwater network.